CIMAC CONGRESS 25
ZURICH, MAY 19 – 23, 2025

2025 | 196

Study of Main Engine Behavior During Rough Seas Based on Ship Monitoring Data

Controls, Automation, Measurement, Monitoring & Predictive Maintenance

Rei Miratsu, Nippon Kaiji Kyokai (ClassNK)

Michio Takagi, Nippon Kaiji Kyokai (ClassNK)
Yuzhong Song, Nippon Kaiji Kyokai (ClassNK)
Junshi Takashina, Nippon Kaiji Kyokai (ClassNK)
Takuya Wako, Nippon Kaiji Kyokai (ClassNK)
Koji Takasaki, Kyushu University & Technical Advisor, Nippon Kaiji Kyokai (ClassNK)

ABSTRACT

As the maritime industry is undergoing a profound transformation to decarbonize and achieve the International Maritime Organization's (IMO) ambitious net-zero emissions goal by 2050, various digital technologies, such as advanced data analysis and Condition Monitoring (CM) have been explored in order to quantify ship performance, particularly the main engine's performance. A thorough analysis of the navigation data of a bulk carrier by the authors has revealed huge potential for fuel savings and improving the main engine's reliability. The analysis results show main engine's fuel efficiency was significantly reduced when the ship encountered rough seas. This study provides groundbreaking insights on the relation between the main engine performance and the sea states and how it can be used to improve the ship's operational efficiency and the safety as well.

This study employs a methodology that estimates encountered sea states by integrating ship position and time data with wave hindcast data. These estimated sea states are then correlated with various measured parameters, including main engine power, main engine speed, fuel consumption, and navigation data such as log speed. The power curves of the vessel are calculated based on conventional theoretical equations and the latest analytical methods, and compared with the measured data. Through these comparisons, the gap between current analytical methods and real-world phenomena can be elucidated.

The data utilized in this study comprise detailed measurements of main engine performance, voyage logs, and wave hindcast data. This robust dataset facilitates an in-depth examination of the interplay between sea conditions and engine behavior. The findings reveal significant correlations between the severity of encountered sea states and variations in engine performance metrics, such as increased fuel consumption and fluctuations in engine speed. Under specific conditions, such as wave direction, a certain positive correlation was confirmed between the conventional theoretical-based power curve and the relationship between ship speed to water and main engine power calculated from measured values. This suggests that conventional simulations can accurately prepare power curves according to the encountered sea conditions.

This research uncovers previously uncharted aspects of main engine behavior in rough seas, highlighting the practical applications of these findings. By identifying and quantifying the impact of rough sea conditions on engine performance, this study lays the foundation for developing advanced maintenance protocols and more efficient navigation strategies. These insights are not only innovative but also crucial for reducing the environmental footprint of maritime operations through enhanced fuel efficiency.

In conclusion, this study significantly contributes to the maritime industry by providing a detailed quantitative analysis of main engine behavior during rough seas. The insights gained from this research are expected to drive advancements in CM and support the implementation of energy-saving measures. By bridging a critical knowledge gap, this study paves the way for more resilient and sustainable maritime practices, underscoring the transformative potential of integrating real-world data into engine performance analysis and operational decision-making.

1 INTRODUCTION

The maritime industry is undergoing a significant transformation toward decarbonization in order to achieve the ambitious net-zero emission target set by the International Maritime Organization (IMO) by 2050 [1]. This shift has prompted extensive consideration of various digital technologies, such as advanced data analysis and condition monitoring (CM), aimed at quantitatively assessing ship performance and safety, particularly the performance of main engines. In recent years, efforts to monitor ship propulsion systems have expanded to evaluate propulsion performance and safety in actual sea conditions [2][3].

The integration of vessel position data with wave hindcasting, which can estimate wave conditions at any given time and location globally, enables accurate comprehension of the encountered sea state for ships. Understanding the encountered sea state is essential for evaluating propulsion performance in actual seas, and analyzing the encountered sea state data alongside in-situ ship measurements allows for a quantitative understanding of the phenomena occurring under actual operating conditions. Previous studies have demonstrated trends in speed reduction of ships in the North Atlantic, with significant decreases in speed observed under conditions of head seas, oblique seas, and beam seas as significant wave height increases, as shown in Figure 1 [4]. However, these studies do not classify whether the observed speed reductions are due to intentional slowdowns by the captain or natural speed losses caused by increased resistance in rough seas.

Additionally, recent advancements have enabled estimations of hull resistance under actual sea conditions that take into account wave conditions [5]. Based on the estimated hull resistance, propeller characteristics can be applied to calculate the torque required as a load on the main engine. With an appropriate main engine model, the main engine's response to the load can also be estimated. Simulations that consider the interactions among hull resistance, propeller characteristics, and the main engine have been extensively studied in previous research [6] Notably, the cycle mean value model allows for rapid calculations, enabling near-real-time understanding of the behavior and performance of individual components within the ship's propulsion system [7].

This paper investigates ship speed reduction and main engine behavior under severe sea conditions by combining actual ship measurement data with encountered wave data. Furthermore, a propulsion system model simulating the actual vessel was developed by integrating hull resistance calculated through OCTARVIA, a tool developed by Japan's JIP, with the MVEM model from previous studies [5]. Validation of the model was conducted through comparison with actual ship measurement data.

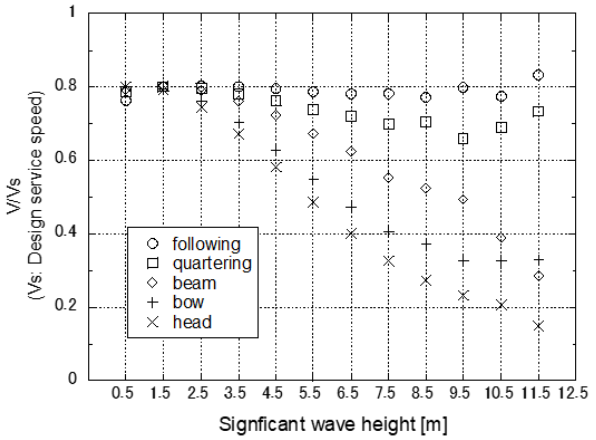

Figure 1. Average ship speeds in each encountered wave height and wave headings (Bulk carriers, oil tankers and container ships)

2 FULL-SCALE MEASUREMENT

This study utilizes 124 days of operational measurement data collected from a Panamax bulk carrier. Table 1 provides an overview of the data used in this article. Main engine output was estimated based on fuel consumption and engine speed, with hourly averages applied to main engine output, engine speed, and the Fuel Indicator. Due to confidentiality, these parameters were normalized using shop test data.

From the voyage data, speed through water, heading, and latitude/longitude were used. Speed through water was normalized using the service speed. The encountered sea state was estimated by associating vessel position and time data with oceanographic data on an hourly basis. The sea state data were sourced from the ERA-5 wave hindcast dataset provided by the European Centre for Medium-Range Weather Forecasts (ECMWF) [8]. The relative wave direction against the vessel was determined by calculating the angle between the headings and the mean wave direction.

Table 1. Overview of data used in this study.

Data	Contents	Sampling period
Voyage	Log speed, Course over ground, Latitude, Longitude	1 hour
Main Engine	Engine speed, Engine speed command, Engine Output, Fuel indicator	1 min
Wave	Significant wave height, Wave period, Wave direction	1 hour

3 MODEL OF PLOPULSION SYSTEM

In this study, the Mean Value Engine Model (MVEM) is used to handle settings and control modes aimed at optimizing engine operation according to different operational conditions and objectives. To enhance computational efficiency, the model averages cycle fluctuations without considering the behavior of individual engine cylinders. Each component model—hull resistance, propeller, and engine—was developed and integrated using MATLAB Simulink. The equations of motion used in this model are presented below. As shown in Figure 2, The coordinate system is defined with the origin at the center of the ship on the water surface, following a right-handed system in which the positive x-axis points forward in the direction of the ship, and the positive z-axis points upward.

$$(m + m_x)\dot{u} = X_{Hull} + X_{Propeller} + X_{Wave} + X_{Wind}$$

$$2\pi(I_P + J_P)\dot{n} = Q_P + Q_E$$

where m and m_x are the mass of the ship and the added mass of the ship in the x-direction, u is the velocity of the ship in the x-direction, X_{Hull} , $X_{Propeller}$, X_{Wave} and X_{Wind} are the longitudinal forces acting on the ship due to the hull, propeller, wind pressure, and waves, I_P is the polar moment of inertia of propeller, J_P is the added water inertia moment of the propeller and Q_E and Q_P are the engine and propeller torques.

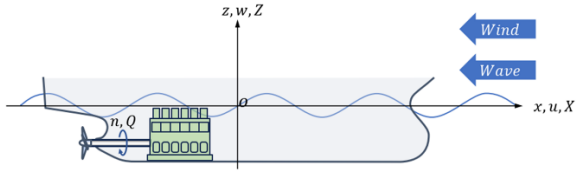

Figure 2. Coordinate system in this study.

3.1 Engine

In this study, an MVEM approach is adopted [7]. The engine crankshaft speed N_E and turbocharger shaft speed N_{Tc} are calculated using the following equations, derived by applying angular momentum conservation to the propulsion plant shaft system and the turbocharger shaft, respectively:

$$\frac{dN_E}{dt} = \frac{30(\eta_{Sh}Q_E - Q_P)}{\pi(I_E + I_{Sh} + I_P)}$$

$$\frac{dN_{Tc}}{dt} = \frac{30(Q_T - Q_C)}{\pi I_{Tc}}$$

where Q_E and Q_P are the engine and propeller torques, I_E , I_{Sh} and I_P are the polar moment of inertia of engine, shafting system and propeller, respectively, η_{Sh} is the shafting system efficiency, Q_C and Q_T are the compressor and turbine torques, I_{Tc} are the turbocharger rotating parts polar moment of inertia.

The model was tuned using the results of the engine shop test for a Panamax bulk carrier. As shown in Table 2, the main engine speed, main engine output, and turbocharger speed at 50% load and 100% load were confirmed to be within a 3% error margin.

The flow of fluid within the cylinder is assumed to be continuous for the calculation. The relationship between the flow rates at the cylinder inlet and outlet is expressed by the following equation:

$$m_a + m_f = m_e$$

where m_a, m_f and m_e are the mass flow rate of air, fuel and exhaust gas.

For example, the fuel flow rate m_f is expressed by the following equation, considering the number of cylinders Z_{cyl}, the fuel injection quantity per cycle $m_{f,\ cy}$, engine speed N_e and rev_{cy} (where 2st = 1, 4st = 2). The fuel flow rate in Figure 3 is compared with the results from the shop test, and the error under the current conditions is less than 0.1%.

$$m_f = \frac{Z_{cyl} m_{f,\ cy} N_e}{60 rev_{cy}}$$

Table 2 Comparison between the simulation results (Engine speed, Engine output, Turbocharger speed) at 50% and 100% engine load and the shop test data.

Load	Error [%]		
	Engine speed	Engine output	Turbocharger speed
50 %	0.00	1.39	2.23
100%	1.37	2.90	1.73

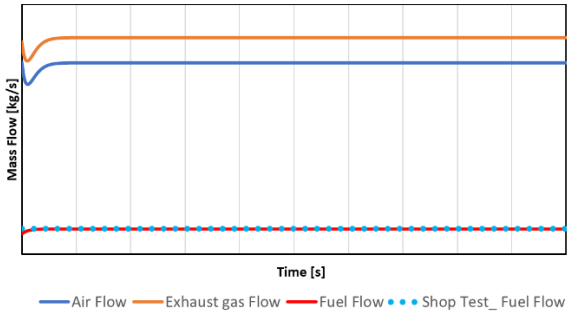

Figure 3. Comparison between the simulation results (mass flow rates of air, fuel, and exhaust gas) and the engine's shop test (mass flow rate of fuel).

3.2 Hull

In the model developed in this study, the longitudinal force on the hull is defined as follows. The total resistance coefficient C_T takes into account factors including frictional resistance, pressure resistance, added resistance in waves, air resistance, and hull roughness.

$$X_{Hull} = -R_T$$

$$C_T = \frac{R_T}{\frac{1}{2}\rho S_W u^2}$$

Where R_T is the hull resistance, ρ is the density of sea water and S_W is the wetted surface area.

The following formula was used to calculate the wind pressure. The wind pressure coefficient C_{XW} is obtained from Octarvia.

$$X_{Wind} = C_{XW}(\alpha_W)\frac{1}{2}\rho_A A_F V_W^2$$

Where α_W is the relative wind direction, ρ_A is the density of air, A_F is the frontal area of the hull above the waterline and V_W is the relative wind speed.

For the longitudinal force due to waves, both the wave excitation force X_{W1} and the added resistance in waves X_{W2} are accounted for, as shown in the following equations.

$$X_{Wave} = X_{W1} + X_{W2}$$

The wave excitation force, also known as the first-order force, refers to a periodic fluctuating force proportional to wave amplitude. In this study, the Froude-Krylov force $C_{W1}(\omega)$ related to surge was calculated using a simplified equation [9]. The longitudinal force acting on the ship was considered in this analysis.

$$X_{W1} = C_{W1}(\omega)\rho g L B \zeta_a \sin \omega t$$

Where g is the gravitational acceleration, L and B are the ship length and breath, ζ_a is the wave amplitude and ω is the regular wave frequency.

The increase in resistance due to wave conditions was derived from the following equation. The irregular wave resistance increase coefficient C_{W2} was calculated using Octarvia.

$$X_{W2} = C_{W2}(T_w, u, \beta) 8 \rho g H_W^2 \left(\frac{B^2}{L}\right)$$

Where T_w is the mean wave period, β is the wave headings and H_w is the significant wave height.

Figure 4 presents an example of the simulation results, and Figure 5 indicates the definition of wave headings. In the simulations, the engine speed command was kept constant, while only wave height, wave direction, wind speed, and wind direction were varied.

Notably, under head seas, an increase in wave height resulted in a reduction in ship speed, whereas no significant deceleration was observed under following seas, even as wave height increased. This trend aligns with the statistical data on actual ship speed reduction shown in Figure 1, confirming that the effects of wave height and wave direction have been accurately modeled in the simulations.

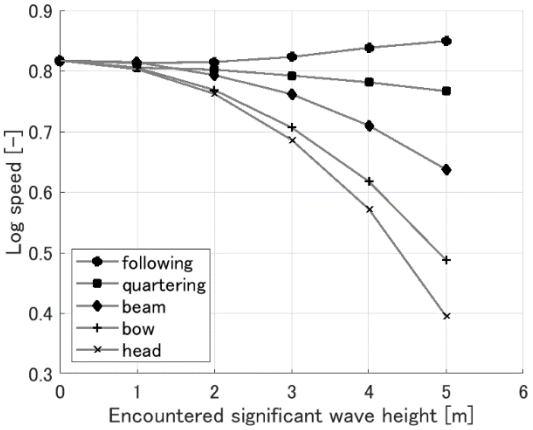

Figure 4. Example of simulation results for encountered significant wave height, wave headings and log speed.

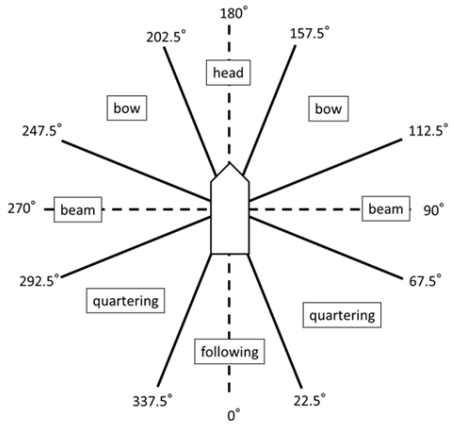

Figure 5. Definition of wave headings.

3.3 Propeller

The longitudinal force generated by the propeller is defined by the following equation. The thrust coefficient K_T and the torque coefficient K_Q were calculated from the chart of the MAU-type propeller [10].

$$X_{Propeller} = (1-t)T_P$$

$$T_P = K_T(J)\rho n^2 D^4$$

$$Q_P = K_Q(J)\rho n^2 D^5$$

$$J = \frac{u_a}{nD}$$

Where t the thrust deduction factor, T_P is the propeller thrust, Q_P is the propeller torque, n is the propeller rotational speed, D is the propeller diameter, J is the propeller advance coefficient and u_a is the inflow velocity to the propeller. The variation in the inflow velocity to the propeller considers the effects of orbital velocity.

Figure 6 presents an example of simulation results for propeller torque. The simulation conditions are identical to those in Figure 4. Notably, under head sea conditions, an increase in wave height corresponds to an increase in propeller torque. In contrast, under following sea conditions, no significant increase in propeller torque is observed with increasing wave height.

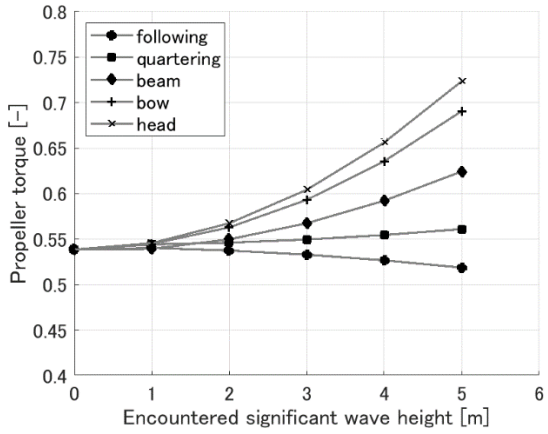

Figure 6. Example of simulation results for encountered significant wave height, wave headings and propeller torque.

4 RESULTS AND DISCUSSIONS

4.1 Speed Reduction in Actual Operating Conditions

The measurement data from the ship were organized based on the encountered wave height and wave direction in order to examine the quantitative relationship between sea conditions and the behavior of the propulsion system.

4.1.1 Relationship Between Encountered Significant Wave Height and Log Speed

Figure 7 shows the relationship between the log speed and engine output at full load condition and the encountered significant wave height. For vessels navigating in actual seas, resistance arises not only from the resistance experienced in calm waters but also from waves, wind and other factors. In particular, the influence of resistance due to waves is significant. As shown in Figure 7, an increase in encountered significant wave height corresponds to a decrease in ship speed, even though the main engine output remains constant. Figure 8 shows the results of Figure 7 categorized by wave heading. Significant deceleration is observed with an increase in wave height for head seas, bow seas, and beam seas, while no deceleration is observed with an increase in wave height for following seas.

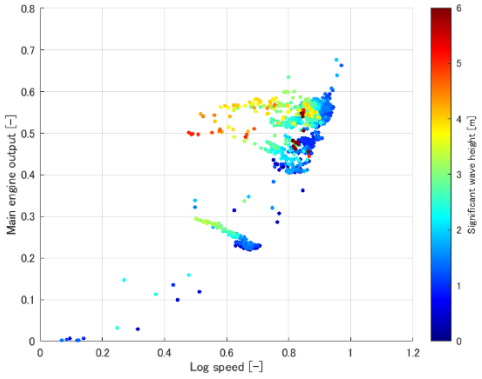

Figure 7. The relationship between main engine output, log speed, and encountered significant wave height.

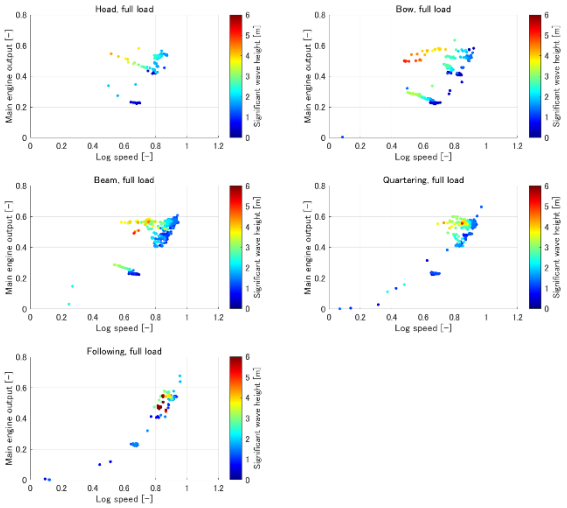

Figure 8. The relationship between main engine output, log speed, and encountered significant wave height for each wave heading.

4.1.2 Detailed Analysis of a Single Voyage

The relationship between encountered sea conditions and speed reduction was examined in detail through an analysis of measurement data from a single voyage.

During this voyage, the ship encountered significant wave heights exceeding 4 meters a total of four times. Table 3 assigns numbers (1) through (4) to each event and summarizes the wave data and each measured data. Figure 9 presents the time-series data for the main engine output, log speed, engine speed, engine speed command and fuel indicator. The color of the plot represents the encountered significant wave height, with the color gradient from blue to red indicating an increase in wave height.

During event (1), the wave direction was head seas, and as the encountered significant wave height increased, both the main engine output and the Fuel Indicator increased, while the log speed decreased. This is believed to be caused by the increased hull resistance in the waves due to the rising significant wave height in head seas. Event (2) represents the largest encountered significant wave height, 6.5 meters, but since the wave direction was following seas, although the engine speed was temporarily reduced, there was no decrease in ship speed. In event (3), the ship encountered a combination of beam seas and oblique head seas. Although the engine speed was reduced, the ship was unable to maintain the lower engine speed due to the increased wave resistance, leading to a significant reduction in log speed. Additionally, to maintain the engine speed, the Fuel Indicator remained at high values for a relatively long period. Event (4) involved beam seas, but similar to event (1), as the encountered significant wave height increased, both the main engine output and the log speed decreased.

Table 3. The summary of encountered sea conditions and measurement data for each event.

No.	Wave height [m]	Wave direction	Engine output	Log speed	Engine speed	Engine speed command
(1)	4.5	Head	0.54	0.56	0.79	0.79
(2)	6.5	Follow	0.47	0.83	0.81	0.81
(3)	5.0	Beam, Bow	0.49	0.48	0.77	0.79
(4)	4.0	Beam	0.57	0.63	0.84	0.84

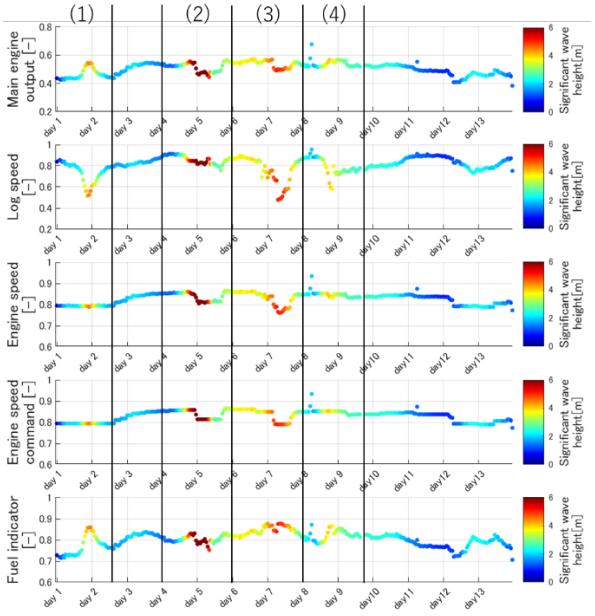

Figure 9. Time series data of main engine output, log speed, engine speed, engine speed command and fuel indicator.

Figures 10 through 13 show the relationship between log speed and main engine output for each event. In Event (1), under head sea conditions with a constant engine speed, an increase in significant wave height tends to result in increased main engine output and decreased ship speed. However, in Event (2), with following sea conditions, no notable deceleration with increasing significant wave height, as observed in Event (1), occurs. In Event (3), under beam and oblique seas, a moderate reduction in set engine speed is observed, with corresponding decreases in both main engine output and ship speed. In Event (4), under beam sea conditions with constant engine speed, a trend of deceleration with increasing significant wave height is also evident.

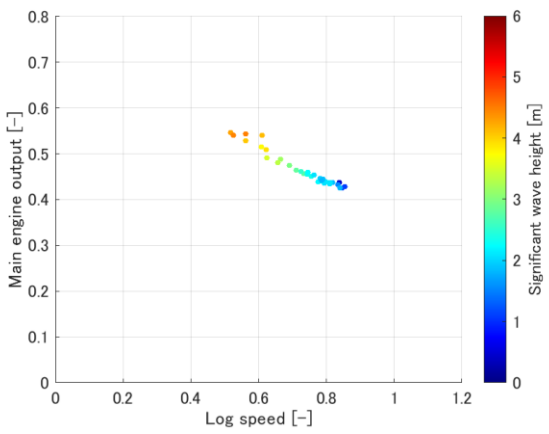

Figure 10. Relationship among main engine output, log speed, and fuel indicator in event (1).

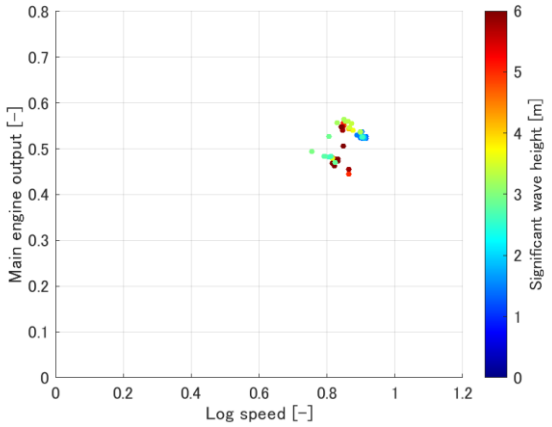

Figure 11 Relationship among main engine output, log speed, and fuel indicator in event (2).

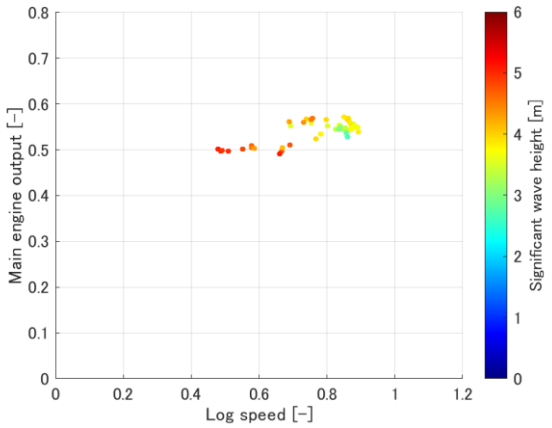

Figure 12. Relationship among main engine output, log speed, and fuel indicator in event (3).

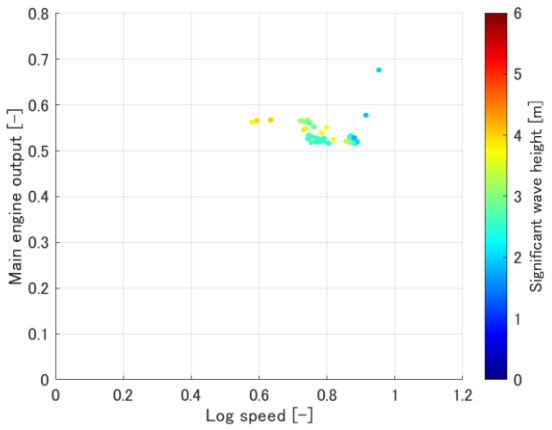

Figure 13. Relationship among main engine output, log speed, and fuel indicator in event (4).

4.2 Validation of the Propulsion Model Using Full-Scale Measurement Data

The validity of the model was verified by conducting simulations with the 1D model using the encountered wind and sea conditions as well as the actual engine speed from Events (1) through (4) in Section 4.1.2 as input values, and comparing the analysis results with the measurement data.

Figures 14 to 17 show the comparison between the measured values and simulation results for each event. The measured values are represented by circles, while the simulation results are shown as squares. The color of each plot indicates the magnitude of the significant wave height. The simulation was performed by sampling data from representative times for each event, using the actual engine speed and resistance coefficients corresponding to the wave conditions (wave height, period, wave heading), along with the ship speed and loading condition as inputs.

Event (1) refers to a case where the wave height increased while the ship was encountering head seas with a constant engine speed command. The simulation results successfully reproduced the trend of increased main engine output and decreased ship speed with the increase in wave height, consistent with the measured values. The maximum error between the simulation results (4 points) and the measured values was 7.9 % for ship speed and 4.2 % for output.

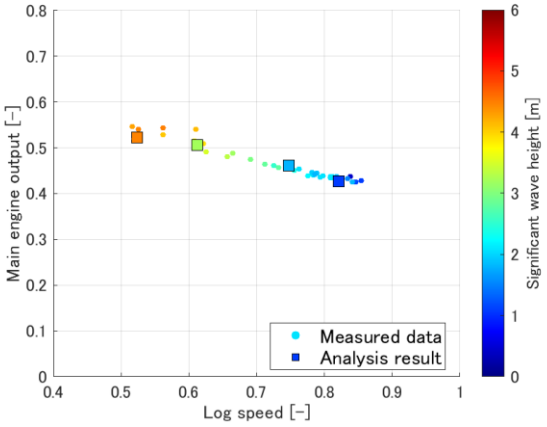

Figure 14. Comparison of full-scale measurements and simulation results for event (1).

Event (2) refers to a case under following sea conditions where the wave height increased, and the engine speed was reduced by one step. After the reduction in engine speed, higher wave heights resulted in lower output but higher ship speed, and a trend of increasing output and ship speed was observed as wave height decreased. This can be attributed to the fact that, under following sea conditions, an increase in wave height does not necessarily contribute to an increase in wave-induced resistance. However, the simulation results did not replicate these qualitative trends, indicating the need for further investigation.

It should be noted that Event (2) was not purely following seas but included conditions of oblique following seas. Moreover, the irregular wave resistance increase coefficient used in this study has a 30-degree interval for wave direction. As a result, the simulation input used the following sea coefficient, which may be one of the causes of the error. The maximum error between the simulation results (5 points) and the measured values was 3.6 % for ship speed and 5.7 % for output.

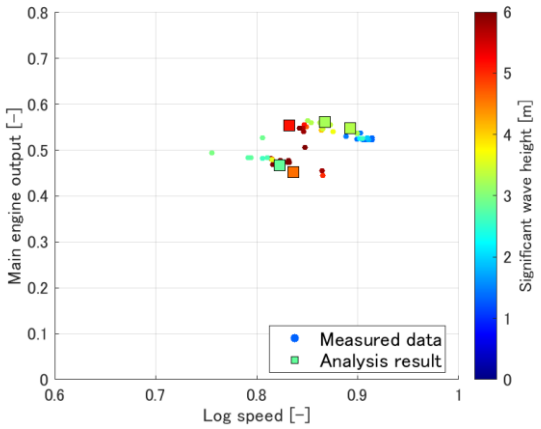

Figure 15. Comparison of full-scale measurements and simulation results for event (2).

Event (3) refers to a case under conditions of beam seas transitioning to bow seas, where the wave height increased and the engine speed was reduced by one step. The qualitative trends in main engine output and ship speed for each engine speed were successfully replicated in the simulation. The maximum errors between the simulation results (5 points) and the measured values were 9.1 % for ship speed and 3.5 % for output.

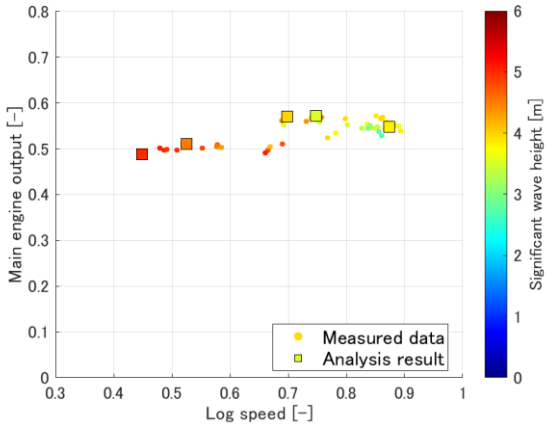

Figure 16. Comparison of full-scale measurements and simulation results for event (3).

Event (4) corresponds to a scenario under beam sea conditions with an increase in wave height, where the commanded engine speed remained constant. The simulation results generally showed a correlation with the measured values. The errors between the simulation results (4 data points) and the measured values were up to 3.1 % for ship speed and 5.0 % for engine output.

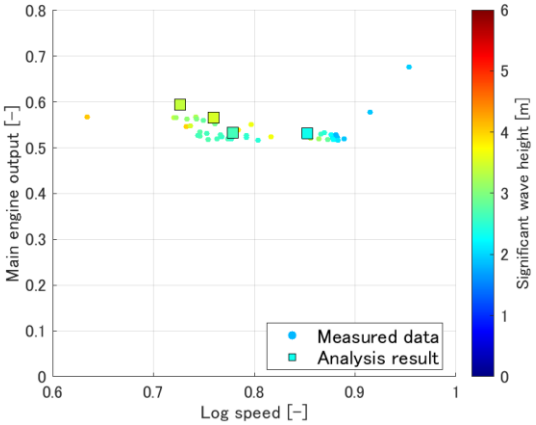

Figure 17. Comparison of full-scale measurements and simulation results for event (4).

5 CONCLUSIONS

Based on analyzing the actual ship measurement data and wave hindcast data, the behavior of the main engine during encounters with rough weather was quantitatively assessed. Specifically, in head seas, a notable decrease in speed and an increase in main engine output were observed as the encountered wave height increased. In contrast, in following seas, no significant deceleration or increase in output was observed with the increase in encountered significant wave height. These findings suggest that the influence of wave heading is a key factor affecting deceleration and the main engine's performance during rough weather encounters.

Furthermore, the validity of the 1D simulation model for the propulsion system, developed in this study, was verified through comparisons with the measurement data. A total of four events with different wave headings were compared, and while the number of comparison points was limited, it was confirmed that the propulsion system's state during rough weather encounters could be estimated with a maximum error of 9.1 % in ship speed and 5.7 % in output. Although further accuracy validation is required, the 1D simulation model has demonstrated the potential for future application in assessing the propulsion system's state under various environmental conditions, which could contribute to enhancing propulsion system safety and supporting more efficient operations.

Future work will involve comparing measurement data and estimated values across multiple additional events to conduct a more comprehensive accuracy validation of the developed model. Additionally, methods such as data assimilation will be explored to improve estimation accuracy. Further studies will also examine whether the deceleration behavior under rough weather conditions and the reproduction of actual propulsion system performance can be achieved using the 1D model for other ship types.

6 ACKNOWLEDGMENTS

The author would like to express sincere gratitude to Professor Theotokatos of Strathclyde University for his invaluable guidance and insightful advice regarding the development of the MVEM model.

7 REFERENCES AND BIBLIOGRAPHY

[1] International Maritime Organizations. 2023. 2023 IMO Strategy on Reduction of GHG Emissions from Ships, RESOLUTION MEPC.377(80).

[2] Tera, T., Iima, S. and Wako, T. 2022. CBM Life Cycle Maintenance, ClassNK Technical Journal No.5 2022 (I): 101-107.

[3] ClassNK, 2021. CBM Guidelines (Edition 2.0).

[4] Miratsu, R., Fukui. T., Matsumoto, T. and Zhu, T. 2020. Study on Ship Operational Effect for Defining Design Values on Ship Motion and Loads in North Atlantic, ASME 2020 39th International Conference on Ocean, Offshore and Arctic Engineering.

[5] Tsujimoto, M., Sogihara, N., Sato, H., Kume, K., Orihara, H., Sugimoto, Y. and Kuroda, M. 2020. Development on Performance Evaluation of Ships in Actual Seas - OCTARVIA Project -, Proc. of HullPIC2020: 54-63.

[6] Mizythras, P., Boulougouris. and Theotokatos, G. 2018. Numerical study of propulsion system performance during ship acceleration, Ocean Engineering 149(2018): 383-396.

[7] Theotokatos, G. 2010. On Cycle the Mean Value Modelling of Large Two-Stroke Marine Diesel Engine, Proceedings of the Institution of Mechanical Engineers Part M Journal of Engineering for the Maritime Environment.

[8] Hersbach, H., Bell, B., Berrisford, P., Hirahara, S., Horanyi, A., Munoz-Sabater, J., et al. 2020. The ERA5 global reanalysis. Q J R Meteorol Soc 146:1999–2049.

[9] Matsui, S., Shinomoto, K., Sugimoto, K. and Ashida, S. 2021. Development of Simplified Formula of Froude-Krylov Force of 6-DOFs Acting on Monohull Ship, ClassNK Technical Journal No.3 2021 (I): 93-112.

[10] Yazaki, A., Takahashi, M. and Minakata, J. 1960. Open Water Test Series with Modified AU-Type Four Bladed Models, Journal of Zosen Kyokai, SNAJ 108.